

Fast and slow edges in bilayer graphene nanoribbons: Tuning the transition from band- to Mott-insulator

Alberto Cortijo, László Oroszlány, and Henning Schomerus
Department of Physics, Lancaster University, Lancaster, LA1 4YB, United Kingdom
(Dated: November 16, 2018)

We show that gated bilayer graphene zigzag ribbons possess a fast and a slow edge, characterized by edge state velocities that differ due to non-negligible next-nearest-neighbor hopping elements. By applying bosonization and renormalization group methods, we find that the slow edge can acquire a sizable interaction-induced gap, which is tunable via an external gate voltage V_g . In contrast to the gate-induced gap in the bulk, the interaction-induced gap depends non-monotonously on the on-site potential V .

PACS numbers: 73.20.At,73.21.-b,71.10.Pm,81.05.Uw

I. INTRODUCTION

One of the most attractive properties of bilayer graphene (which is made of two coupled atomic layers of carbon) is the ability to induce a tunable spectral gap Δ_V by applying a perpendicular electric field.¹⁻⁵ Rapid advances in patterning graphene on the nanoscale now make it feasible to fabricate graphene ribbons with well defined edge termination,^{6,7} while experiments on narrow ribbons show that they can display a gap Δ_W due to transverse size quantization.⁸ The ensuing facility to confine electrons in a controllable way via gate potentials and patterning makes bilayer nanoribbons a promising candidate for nanoelectronic applications. Systems suitable of being used as a basis for a transistor should exhibit a high resistance in the off state. In the case of nanoribbons with zigzag termination, however, this requirement poses a problem, since the edges support current-carrying states with energies inside the bulk gap, and a much reduced hybridization gap $\Delta_h \ll \Delta_V, \Delta_W$ due to exponentially small tunneling between the edges.⁹⁻¹² On the other hand, several novel concepts (notably, valleytronics¹³) exploit the existence and specific properties of such edge states.

Previous works on edge states in gated bilayer ribbons ignore two elements: (i) next-nearest-neighbor hopping, which is known to strongly affect the bulk properties¹⁴⁻¹⁶ and is of crucial importance for edge states in monolayer ribbons,¹⁷ and (ii) the effects of interactions, which are known to strongly influence the properties of quasi-one dimensional systems, including carbon-based systems.^{18,19} In this paper, we point out that next-nearest-neighbor hopping breaks the symmetry between the edges, resulting into a slow edge and a fast edge characterized by different values of the propagation velocity. We then explore the consequences for the question whether many-body effects can help to open a gap in these channels. Treating interactions in a Hubbard model on the basis of bosonization and renormalization group methods at $T = 0$, we find that the edge channels display a Mott transition at half filling. In presence of the higher-order hopping terms, the associated charge gap Δ_ρ on the slow

edge can take on sizeable values, while on the fast edge the gap is negligibly small. Remarkably, the gap depends sensitively on the applied gate voltage V ; the effects of interactions can therefore be controlled externally. Furthermore, the dependence of Δ_ρ on V is non-monotonic, in striking contrast to the behavior of the field-induced gap Δ_V in the bulk of the system.

This paper is organized as follows. In Sec. II we present the hamiltonian for the graphene bilayer ribbon including the next-nearest-neighbor hopping and the hopping term between non-dimerised atoms in both layers. We then describe the edge states for a zigzag ribbon of bilayer graphene and their different localization properties along the transverse direction of the ribbon by computing the Inverse Participation Ratio. In Sec. III we describe the effects of considering electron-electron interactions in the spectrum for edge states. We find that because the different properties of the two edges the gap opened by the interaction is different for both edges. We also briefly discuss a possible experimental verification of this different behavior. We summarize our results in Sec. IV.

II. TIGHT BINDING MODEL

A graphene bilayer nanoribbons with zigzag edge termination is shown in Fig. 1 (left panel). Focussing on the low-energy bands which participate in electronic transport, such ribbons can be modelled by a tight-binding hamiltonian $H = \sum_{\sigma=\downarrow,\uparrow} \sum_{ij} \gamma_{ij} c_{i,\sigma}^\dagger c_{j,\sigma}$, where each carbon atom hosts one spin-degenerate electronic orbital with annihilation operator $c_{i\sigma}$. Recent experiments specifically addressed the values of the parameters γ_{ij} in bilayer graphene.¹⁴⁻¹⁶ Nearest-neighbor hopping in the same graphene layer is described by a hopping element $-\gamma_0$, where $\gamma_0 \simeq 3\text{eV}$. The layers are Bernal stacked, with hopping element $\gamma_1 \simeq 0.12\gamma_0$ between dimerised atoms that lie on top of each other. The symmetry between both layers can be broken by top- or back-gates with a gate voltage V_g , which induce a perpendicular electric field and give rise to an on-site potential $\pm V$ on

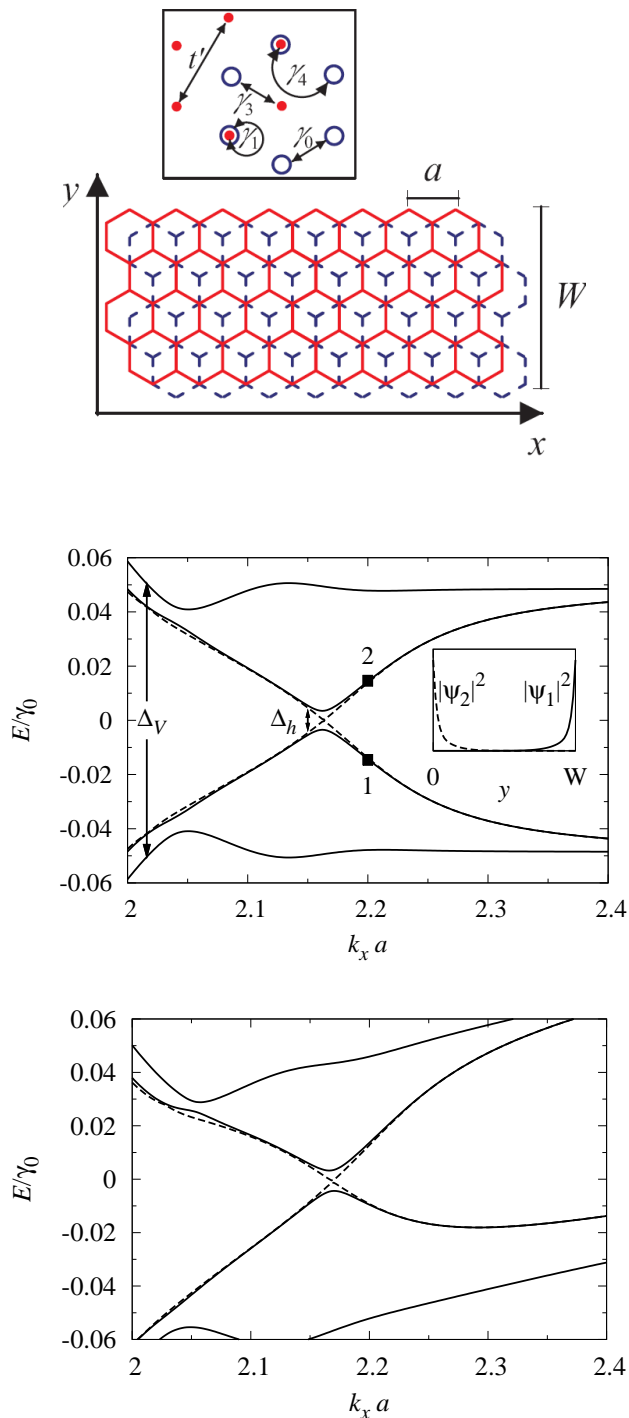


FIG. 1: (Color online) Upper panel: Sketch of a bilayer graphene nanoribbon of lattice constant a and width W (inset: definition of hopping terms). Middle panel: Dispersion relation of edge states for a nanoribbon with $W = 32 \times \sqrt{3}a$ and layer-symmetry breaking potential $V = 0.025 \gamma_0$, focussing on one of the two K points ($k_0 = 2\pi/(3a)$). (Dashed lines: two innermost bands for $W = 40 \times \sqrt{3}a$.) Here we use hopping matrix elements $\gamma_1 = \gamma_3 = 0.12 \gamma_0$, but set $\gamma_4 = t' = 0$. The inset shows the transverse charge distribution of two edge states with energies indicated by the markers. Lower panel: The same but including hopping terms $\gamma_4 = 0.05 \gamma_0$, $t' = 0.07 \gamma_0$.

the two layers, which is obtained from V_g by including the screening in the layers.³ We assume that V is uniform across the system, even near the boundaries, which in reality will be enforced to a good approximation by the proximity of the metallic gate close to the system. At the boundary, we impose standard hard-wall boundary conditions, which amount to setting the wavefunction to zero on lattice sites that lie outside the ribbon.

It is also conventional to include the direct coupling γ_3 between the non-dimerised atoms in both layers.² Ignoring for the moment other hopping terms, a typical dispersion relation of the edge states in a gated ribbon is shown in Fig. 1 (middle panel). Of the four bands of edge states, two are massive, with a gap $\Delta_V \simeq 2|V|$ (the same as for the bulk states), while the other two display a linear dispersion, corresponding to two counter-propagating states which are well localized at opposite edges (see inset). The same scenario is replicated at the other K point in the graphene Brillouin zone, but with the edges interchanged. Therefore, each edge supports two counter propagating state, one from each K point. Notably, to this level of approximation, the propagation velocities on both edges are the same.

The middle and lower panels of Fig. 1 shows how the dispersion changes when the two most prominent additional hopping elements are taken into account: the interlayer hopping $\gamma_4 \approx 0.05 \gamma_0$ between adjacent dimerized and non-dimerized carbon atoms, and the intralayer hopping $t' \approx 0.07 \gamma_0$ between next-nearest neighbors. Both terms break the particle-hole symmetry, which then discriminates the different edges: the terminating atoms live on different layers and therefore possess a different on-site potential. In the dispersion relation, this takes the effect of an additional background velocity, which increases the velocity at one edge (the 'fast edge') while reducing the velocity at the other edge (the 'slow edge'). The dependence of these velocities on the gate potential is shown in the top panel of Fig. 2. The additional hoppings also affect the transverse localization of the edge states. This is shown in the bottom panel in terms of the inverse participation (IPR) $I_{\text{IPR}} = \sum_n |\psi_n|^4$, which is larger the better localized a state is (here, the sum is over the transverse direction of the nanoribbon).

At this point it is important to mention that there are two types of zigzag edge termination in graphene bilayer,¹¹ the so called α and β terminations. When the on site potential V is zero some qualitative differences in the bandstructure can be found in both cases. However when V_g leads to a nonvanishing V in both cases two of the edge bands become gapped (with a gap of the order of V) and the two other bands cross each other around the Fermi points as discussed before for the two types of edge terminations. Also in both cases the asymmetry between the velocities at different edges can be found, being the differences most prominent at the high energy bands. Thus we will not consider any distinction between the two terminations as long as we are only concerned in the physics at small energies around the Fermi points.

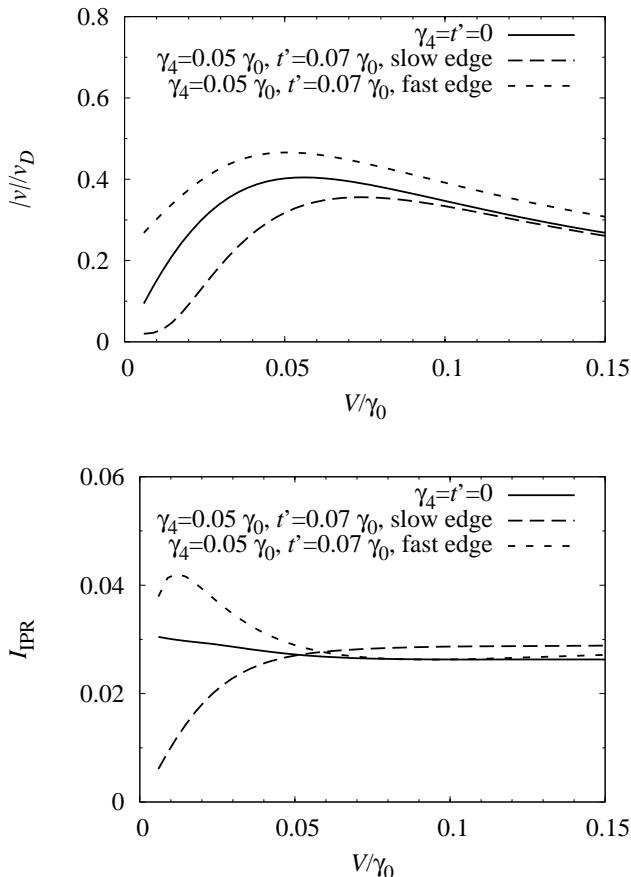


FIG. 2: Influence of γ_4 and t' on the edge-state velocities (top panel, $v_D = \sqrt{3}\gamma_0 a/2\hbar$) and localization on each isolated edge ($\Delta_h = 0$) (bottom panel, expressed in terms of the inverse participation ratio I_{IPR}).

At small energies, the hybridization of the edge states leads to an avoided crossing, where the small residual gap Δ_h vanishes exponentially with increasing width of the ribbon. A sizable hybridization gap Δ_h exists only for small values of W (narrow ribbons). For typical applied gate voltages and widths, each edge of the nanoribbon therefore behaves like a metallic one-dimensional system with two counter-propagating states, where each state is associated to one of the K points. In this scenario of low dimensionality, one should expect that interactions play an important role. Generally, however, interactions are felt most strongly when particles propagate slowly and are well confined. Thus, the concrete manifestations should depend on the distinct properties of the fast and slow edge states described above. This is what we will explore in the remainder of this paper.

III. MANY BODY EFFECTS

Within the tight-binding description, interactions can be incorporated via a Hubbard term $U \sum_i n_{i,\uparrow} n_{i,\downarrow}$, where $n_{i,\sigma} = c_{i,\sigma}^\dagger c_{i,\sigma}$ is the occupation operator on lattice site i with electrons of spin $\sigma = \downarrow, \uparrow$. Assuming $\Delta_h = 0$, each edge can be treated separately via a hamiltonian of non-chiral bosons:

$$H_0 = \sum_{\mu=\rho,\sigma} \int dx \frac{v_\mu K_\mu}{2} \left(\frac{\partial \phi_\mu}{\partial x} \right)^2 + \frac{v_\mu}{2K_\mu} \left(\frac{\partial \theta_\mu}{\partial x} \right)^2, \quad (1)$$

where μ labels the charge (ρ) and spin (σ) sectors, while v_μ and K_μ are the velocity and the Luttinger parameters, respectively. Interaction events that do not lead to backscattering renormalize these parameters in different ways, which yields the usual separation between the spin and charge degrees of freedom²⁰:

$$v_{\rho,\sigma} = \sqrt{\left(v \pm \frac{g_f}{2\pi\hbar} \right)^2 - \left(\frac{g_b}{2\pi\hbar} \right)^2}, \quad (2)$$

$$K_{\rho,\sigma} = \sqrt{\frac{\hbar v \pm \frac{g_f}{2\pi} \mp \frac{g_b}{2\pi}}{\hbar v \pm \frac{g_f}{2\pi} \pm \frac{g_b}{2\pi}}}, \quad (3)$$

where the upper sign applies to ρ , while the lower sign applies to σ .

Most of the interesting physics arises from backward scattering, which leads to a nonlinear Sine-Gordon term in the spin sector,

$$H_{\text{back}} = \frac{g_b}{2\pi^2 a^2} \int dx \cos(\sqrt{8}\phi_\sigma). \quad (4)$$

At half filling, which we need to consider to assess the size of any interaction-induced gap, this is accompanied by umklapp processes, which contribute an analogous term to the charge sector:

$$H_{\text{umklapp}} = \frac{g_b}{2\pi^2 a^2} \int dx \cos(\sqrt{8}\phi_\rho). \quad (5)$$

All these terms are controlled by the forward and backward coupling constants $g_{b,f}$, which are obtained by writing the Hubbard interaction term $U n_{i,\uparrow} n_{i,\downarrow}$ in the basis

$$\Psi(x, y) \sim \varphi_-(y) e^{-ik_0 x} L(x) + \varphi_+(y) e^{ik_0 x} R(x) \quad (6)$$

of the diagonalized one-particle hamiltonian around each K point ($k_0 = 2\pi/(3a)$):

$$g_f = U a^2 \int dy |\varphi_\pm(y)|^2 |\varphi_\pm(y)|^2, \quad (7a)$$

$$g_b = U a^2 \int dy |\varphi_\pm(y)|^2 |\varphi_\mp(y)|^2. \quad (7b)$$

The left-right symmetry of the system results in the additional constraint $g_f = g_b = g = U a I_{\text{IPR}}$, which involves the IPR of the transverse wavefunction. As seen

above, as soon as γ_4 and t' are taken into account the IPR strongly depends on the layer-symmetry breaking potential V . Thus, the effective strength of interactions can be controlled by the applied gate voltage.

Since the terms (4) and (5) make the hamiltonian not exactly solvable, we assess their consequences using standard renormalization group (RG) arguments.^{20,21} In first order in g_b , the RG equations for $y_\mu \equiv \frac{g_b}{\hbar\pi v_\mu}$ and K_μ are

$$\frac{dK_\mu}{dl} = -\frac{y_\mu^2}{2}, \quad \frac{dy_\mu}{dl} = (2 - 2K_\mu) y_\mu, \quad (8)$$

where l is a logarithmic renormalization scale. The scaling behavior of y_μ depends on the value of K_μ . For $K_\mu > 1$, y_μ decreases when the scaling parameter l increases, which renders the interaction term irrelevant. For $K_\mu < 1$, however, the interactions are relevant; the intermediate case $K_\mu = 1$ represents a quantum critical point.

Because of the constraint $g_f = g_b = g$, the Luttinger parameter (3) can be written as

$$K_\rho = \sqrt{\frac{1}{1 + \frac{g}{\pi\hbar v}}}, \quad K_\sigma = \sqrt{\frac{1}{1 - \frac{g}{\pi\hbar v}}}. \quad (9)$$

For the case $g > 0$ (repulsive interactions), to which we restrict our attention, $K_\sigma > 1$ and the RG equations (8) imply that the spin sector will flow towards the noninteracting theory, with renormalized $K_\sigma^* = 1$ due to the emerging spin-rotation invariance. On the other hand, K_ρ is smaller than one, and therefore the system may acquire a gap in the charge sector. For a more quantitative analysis, we introduce the new variable $x_\rho = 2K_\rho - 2$, so that Eq. (8) takes the form

$$\frac{dx_\rho}{dl} = -y_\rho^2, \quad \frac{dy_\rho}{dl} = -x_\rho y_\rho. \quad (10)$$

In these new variables, the RG equations possess a first integral $A^2 = x_\rho^2 - y_\rho^2 = x_{\rho,0}^2 - y_{\rho,0}^2$, whose value remains constant along the trajectories of the flow, and therefore can be calculated using the bare values $x_{\rho,0}$ and $y_{\rho,0}$. Most importantly, none of the flow lines cross the line $x_\rho = y_\rho$, where $A = 0$. This line constitutes a separatrix between two regimes. For $y_\rho < x_\rho$, y_ρ scales to zero and x_ρ approaches a definite renormalized value x_ρ^* . Physically, this sector of the system is then well described by the noninteracting hamiltonian (1) with renormalized K_ρ^* . For $y_\rho > x_\rho$, however, $y_\rho \rightarrow \infty$ and $x_\rho \rightarrow -\infty$ flow towards strong coupling, where the RG equations are no longer valid. The charge sector then acquires a gap Δ_ρ .

For bare value $|x_{\rho,0}|/y_{\rho,0} \ll 1$, this gap can be estimated using the selfconsistent harmonic approximation,²¹ which exploits that the gap scales with l as $\Delta_\rho = \Delta_0 e^l$, with $\Delta_0 \sim v_\rho \Lambda$. This leads to $\Delta_\rho = \hbar v_\rho \Lambda \left(\frac{4K_\rho y_\rho}{(a\Lambda)^2} \right)^{\frac{1}{2-2K_\rho}}$, where we equate the real-space a cutoff with the lattice constant. The quantity Λ is an ultraviolet cutoff in the momentum space. Since

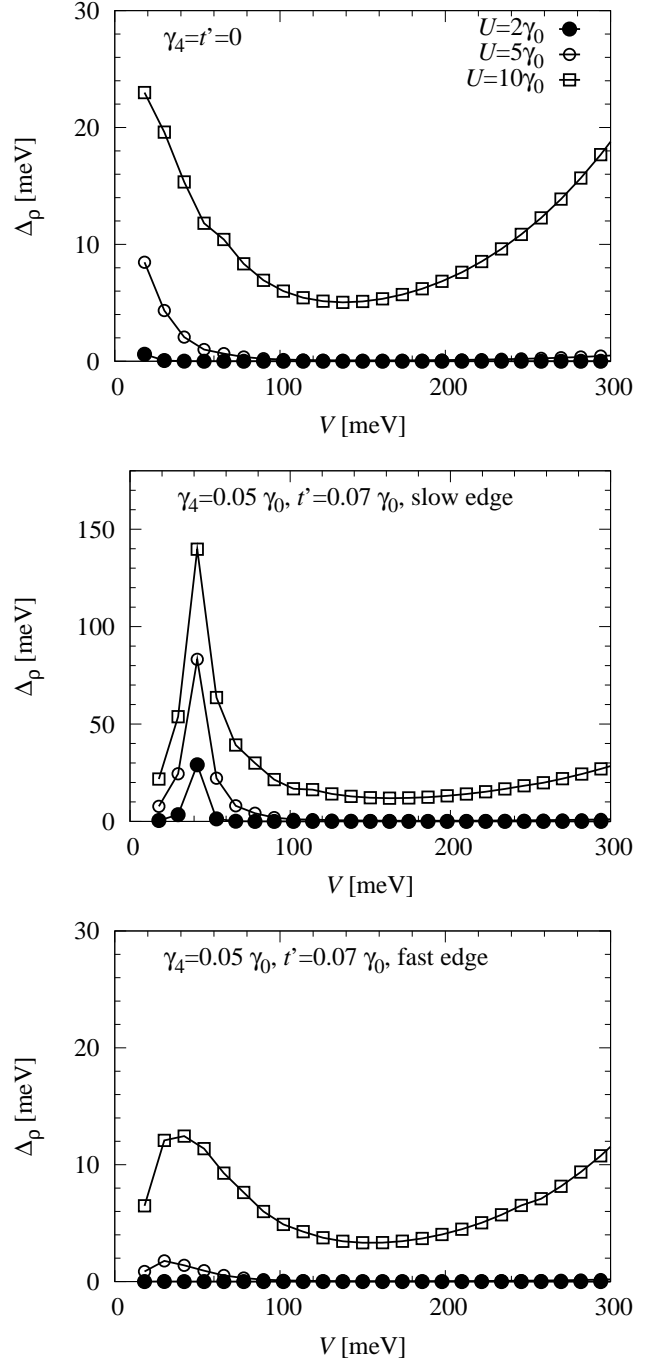


FIG. 3: Charge gap Δ_ρ as a function of V , for selected values of U , assuming $\gamma_4 = t' = 0$ (upper panel), as well as $\gamma_4 = 0.05\gamma_0$, $t' = 0.07\gamma_0$ (middle panel: slow edge; lower panel: fast edge). Note the different scales of the vertical axis.

the edge dispersion relation is linear only for energies less than $\Delta_V \approx 2V$, $\Lambda \sim \frac{2V}{\hbar v_\rho}$, which delivers

$$\Delta_\rho = 2V \left(\frac{K\hbar v_\rho g}{\pi a^2 V^2} \right)^{\frac{1}{2-2K_\rho}}. \quad (11)$$

However, this estimate is only valid when $|x_{\rho,0}| \ll y_{\rho,0} \ll$

1. For $|x_{\rho,0}| \lesssim y_{\rho,0} \ll 1$, the gap must be obtained by terminating the flow at $y_{\rho} \sim 1$, where the first-order expansion breaks down, giving

$$\Delta_{\rho} = 2V\sqrt{1+y_{\rho}}e^{-1/y_{\rho}} = 2V(v_{\rho}/v)e^{-\frac{\pi\hbar v}{g}}. \quad (12)$$

In order to determine which of these regimes applies to the bilayer graphene edge states, we have computed the ratio x/y for some values of V and U . Consistently, $|x_{\rho,0}|/y_{\rho,0} \lesssim 1$, which means that the gap should be obtained from Eq. (12), where v and $g = UaI_{\text{IPR}}$ follow from the results of Fig. 2.

The size of the resulting gap for different scenarios is shown in Fig. 3. In all cases, the dependence of Δ_{ρ} on V is non-monotonic. Ignoring next-nearest-neighbor hopping (left panel), the gap at both edges is identical, but takes a sizeable value only for unrealistically large values of the Hubbard parameter. When γ_4 and t' are taken into account, the gap at the fast edge (right panel) is further suppressed. However, the gap at the slow edge (middle panel) is dramatically increased, in particular in the region where the propagation velocity becomes small.

IV. CONCLUSIONS

We have studied the effect of next-nearest-neighbor hopping and interactions on the edge states in gated bilayer graphene nanoribbons with zigzag termination. The additional hopping results in the formation of a slow and a fast edge, where electrons propagate with different velocities. The small velocity at the slow edge assists the formation of an interaction-induced gap Δ_{ρ} . Whether a sizeable gap can be achieved at realistic interaction

strengths would be best decided by an experiment which exploits that umklapp processes are suppressed when the temperature is raised. The physics behind any experimentally observed gap can therefore be probed via the temperature dependence of the conductivity (measured at the edge via side contacts), which for $T \gg \Delta_{\rho}$ should scale as $\sigma \propto T^{3-4K_{\rho}}$.²² The experimental set up can be a four-terminal geometry which probes each edge separately ($\Delta_h = 0$ and thus the two edges are decoupled for a sufficiently wide nanoribbon). Because each edge state possesses different a different Fermi velocity K_{ρ} is thus different as it is discussed in the text allowing to measure independently each conductivity. This algebraic dependence is distinct from the exponential behavior of the conductivity when the gap originates in the single-particle spectrum (such as the hybridization gap Δ_h due to the finite width of the ribbon). The simultaneous presence of the hybridization gap and interactions could be modelled by a bosonized interaction term $H_{\text{gap}} = -\frac{\Delta_h}{\pi^2 a^2} \sin(\sqrt{8}\phi_{\rho}) \cos(\sqrt{8}\phi_{\sigma})$,^{23,24} which couples the spin- and charge sectors. Moreover, in this situation, right- and left-moving states around the same K point become coupled because of their finite overlap. The fact that these states propagate with different velocities adds interesting complications, which, however, go beyond the scope of the present work.

V. ACKNOWLEDGEMENTS

We gratefully acknowledge discussions with F. Guinea, M. A. H. Vozmediano and G. León Suros and support by the EC via Grant No. MEXT-CT-2005-023778.

¹ T. Ohta et al., *Science* **313**, 951 (2006).
² E. McCann and V. I. Fal'ko, *Phys. Rev. Lett.* **96**, 086805 (2006).
³ E. McCann, *Phys. Rev. B* **74**, 161403(R) (2006).
⁴ E. V. Castro et al., *Phys. Rev. Lett.* **99**, 216802 (2007).
⁵ H. Min, G. Borghi, M. Polini, and A. H. MacDonald, *Phys. Rev. B* **77**, 041407(R) (2008).
⁶ L. Jiao et al., *Nature* **458**, 877 (2009).
⁷ L. C. Campos et al., *Nano Letters* **9**, 2600 (2009).
⁸ M. Y. Han et al., *Phys. Rev. Lett.* **98**, 206805 (2007).
⁹ E. V. Castro et al., *Phys. Rev. Lett.* **100**, 026802 (2008).
¹⁰ J. Rhim and K. Moon, *J. Phys.: Condens. Matter* **20**, 365202 (2008).
¹¹ B. Sahu, H. Min, A. H. MacDonald, and S. Banerjee, *Phys. Rev. B* **78**, 045404 (2008).
¹² M. P. Lima, A. Fazzio, and A. J. R. da Silva, *Phys. Rev. B* **79**, 153401 (2009).
¹³ A. Rycerz, J. Tworzydło, and C. W. J. Beenakker, *Nat. Phys.* **3**, 172 (2007).

¹⁴ L. M. Malard et al., *Phys. Rev. B* **76**, 201401 (2007).
¹⁵ Z. Q. Li et al., *Phys. Rev. Lett.* **102**, 037403 (2009).
¹⁶ A. B. Kuzmenko et al., arXiv:0908.0672.
¹⁷ K. Sasaki, S. Murakami, and R. Saito, *App. Phys. Lett.* **88**, (2006).
¹⁸ C. Kane, L. Balents, and P. A. Fisher, *Phys. Rev. Lett.* **79**, 5086 (1997).
¹⁹ L. Brey and H. A. Fertig, *Phys. Rev. B* **75**, 125434 (2007).
²⁰ T. Giamarchi, *Quantum Physics in One Dimension* (Oxford Science Publications, Oxford, 2003).
²¹ A. O. Gogolin, A. A. Nersesyan, and A. M. Tsvelik, *Bosonization and Strongly Correlated Systems* (Cambridge University Press, Cambridge, 1998).
²² T. Giamarchi, *Phys. Rev. B* **44**, 2905 (1991).
²³ C. M. Varma and A. Zawadowski, *Phys. Rev. B* **32**, 7399 (1985).
²⁴ L. Balents and M. P. A. Fisher, *Phys. Rev. B* **53**, 12133 (1996).